Cell, Vol. 103, 793–803, November 22, 2000, Copyright ©2000 by Cell Press

# Structural Basis for Double-Sieve Discrimination of L-Valine from L-Isoleucine and L-Threonine by the Complex of $tRNA^{Val}$ and Valyl-tRNA Synthetase

**Shuya Fukai,*† Osamu Nureki,*† Shun-ichi Sekine,† Atsushi Shimada,*† Jianshi Tao,‡ Dmitry G. Vassylyev,† and Shigeyuki Yokoyama*†§**

*Department of Biophysics and Biochemistry
Graduate School of Science
The University of Tokyo
7-3-1 Hongo
Bunkyo-ku, Tokyo 113-0033
Japan

†Cellular Signaling Laboratory
Riken Harima Institute at SPring-8
1-1-1 Kohto
Mikazuki-cho, Sayo, Hyogo 679-5148
Japan

‡Cubist Pharmaceuticals, Inc.
24 Emily Street
Cambridge, Massachusetts 02139

## Summary

**Valyl-tRNA synthetase (ValRS) strictly discriminates the cognate L-valine from the larger L-isoleucine and the isosteric L-threonine by the tRNA-dependent "double sieve" mechanism. In this study, we determined the 2.9 Å crystal structure of a complex of *Thermus thermophilus* ValRS, $tRNA^{Val}$, and an analog of the Val-adenylate intermediate. The analog is bound in a pocket, where $Pro^{41}$ allows accommodation of the Val and Thr moieties but precludes the Ile moiety (the first sieve), on the aminoacylation domain. The editing domain, which hydrolyzes incorrectly synthesized Thr-$tRNA^{Val}$, is bound to the 3′ adenosine of $tRNA^{Val}$. A contiguous pocket was found to accommodate the Thr moiety, but not the Val moiety (the second sieve). Furthermore, another Thr binding pocket for Thr-adenylate hydrolysis was suggested on the editing domain.**

## Introduction

High fidelity in protein synthesis is vitally important for all biological systems. The specificity between the amino acid and the codon (the genetic code) critically depends on aminoacylation reactions catalyzed by aminoacyl-tRNA synthetases (aaRSs) (Giegé et al., 1998). The aminoacylation of tRNA proceeds stepwise: (1) the synthesis of an aminoacyl-adenylate, as an active intermediate, from the amino acid and adenosine triphosphate (ATP), and (2) the transfer of the aminoacyl moiety from the adenylate to the 3′-terminal adenosine (3′-A) of tRNA (Fersht and Kaethner, 1976a). The correct recognition of substrates by aaRSs is essential for the accuracy of translation. However, the affinity difference is not large enough for the enzyme to discriminate strictly between similar amino acids (Pauling, 1957). The isoleucyl- and valyl-tRNA synthetases (IleRS and ValRS, respectively) have an editing activity that hydrolyzes incorrect products in a tRNA-dependent manner (Eldred and Schimmel, 1972; Fersht and Kaethner, 1976b; Fersht, 1977, 1985; Freist et al., 1985), while other aaRSs, such as the leucyl-, threonyl-, and alanyl-tRNA synthetases, might also have editing activities to be further characterized (Tsui and Fersht, 1981; Englisch et al., 1986; Freist et al., 1994; Sankaranarayanan et al., 1999, 2000; Cusack et al., 2000). In addition to L-isoleucine, IleRS recognizes and activates L-valine, which is smaller than L-isoleucine by only one methyl group; valyl-adenylate (Val-AMP) is synthesized together with inorganic pyrophosphate ($PP_i$), as shown in Equation 1:

$$\text{IleRS} + \text{L-valine} + \text{ATP} \rightarrow \text{IleRS·Val-AMP} + PP_i \quad (1)$$

Then, IleRS hydrolyzes Val-AMP in a tRNA-dependent reaction:

$$\text{IleRS·Val-AMP} + tRNA^{Ile} \rightarrow \text{IleRS} + \text{L-valine} + \text{AMP} + tRNA^{Ile} \quad (2)$$

This overall reaction of Equation 2 has been shown to comprise two pathways by kinetic analyses (Fersht, 1977, 1985; Freist et al., 1985) and experiments using a DNA aptamer (Hale and Schimmel, 1996). In the "pretransfer editing" pathway, IleRS complexed with $tRNA^{Ile}$ directly hydrolyzes Val-AMP to Val+AMP. When Val-AMP escapes the pretransfer editing, the Val moiety is transferred once to the 3′-end of $tRNA^{Ile}$, and then the synthesized Val-$tRNA^{Ile}$ is hydrolyzed to Val+$tRNA^{Ile}$ by IleRS (the "posttransfer editing" pathway).

In the case of ValRS, the shape and the size of the L-threonine side chain are quite similar to those of L-valine, although one of the methyl groups of L-valine is replaced by a hydroxyl group in L-threonine. ValRS activates this isosteric L-threonine, and forms threonyl-adenylate (Thr-AMP) in addition to L-valine, as shown in Equation 3:

$$\text{ValRS} + \text{L-threonine} + \text{ATP} \rightarrow \text{ValRS·Thr-AMP} + PP_i \quad (3)$$

Then, Thr-AMP is eliminated by the ValRS·$tRNA^{Val}$ complex through the "pretransfer" pathway (Equation 4),

$$tRNA^{Val}\text{·ValRS·Thr-AMP} \rightarrow tRNA^{Val}\text{·ValRS} + \text{L-Threonine} + \text{AMP} \quad (4)$$

and the "posttransfer" pathway (Equations 5 and 6),

$$tRNA^{Val}\text{·ValRS·Thr-AMP} \rightarrow \text{Thr-}tRNA^{Val}\text{·ValRS} + \text{AMP} \quad (5)$$

$$\text{Thr-}tRNA^{Val}\text{·ValRS} \rightarrow tRNA^{Val}\text{·ValRS} + \text{L-threonine} \quad (6)$$

Fersht (1985) proposed the "double-sieve" (two-step substrate selection) model for the mechanism of the amino-acid selection by IleRS: amino acids larger than L-isoleucine are excluded by the aminoacylation site, serving as the "first, coarse sieve," and smaller ones, such as L-valine, are strictly eliminated by the "second, fine sieve" of the putative "editing site." For ValRS, a model analogous to the "double-sieve" model for the

§To whom correspondence should be addressed (e-mail: yokoyama@biochem.s.u-tokyo.ac.jp).

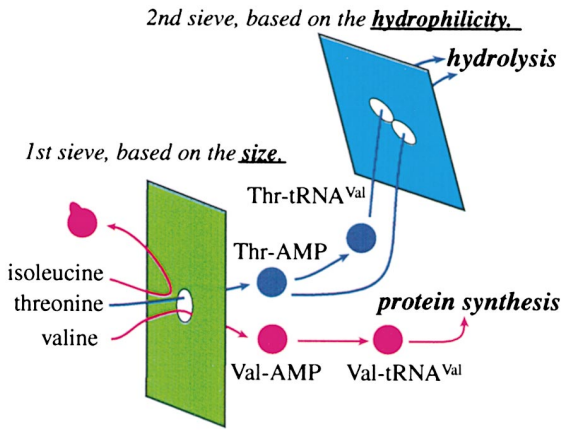


Figure 1. Schematic Drawing of the "Double-Sieve" Concept for Amino Acid Selection by ValRS

IleRS editing has been proposed (Fersht, 1985): L-threonine and L-valine are recognized by the shape in the first step, and L-threonine is discriminated from L-valine by the presence of the hydroxyl group in the second step (Figure 1). In addition to L-threonine, ValRS also activates and edits L-cysteine (Jakubowski, 1980; Jakubowski and Fersht, 1981) and a noncanonical amino acid, L-α-aminobutyrate (Igloi et al., 1977; Fersht and Dingwall, 1979; Jakubowski, 1980), which are smaller than L-valine by one methyl group. The selection mechanism for these two amino acids by ValRS is thought to be similar to that for L-valine by IleRS.

Ten aaRSs, including IleRS and ValRS, constitute class I, while the other ten aaRSs constitute class II (Eriani et al., 1990). The class I aaRSs have a Rossmann-fold domain in common, to catalyze the synthesis of aminoacyl-adenylate and aminoacyl-tRNA, as represented in the crystal structure of *Escherichia coli* glutaminyl-tRNA synthetase (GlnRS) complexed with its cognate $tRNA^{Gln}$ (Rould et al., 1989; Rath et al., 1998). The Rossmann-fold aminoacylation domains of IleRS and ValRS have an insertion (the "connective polypeptide" (CP) domain [Nureki et al., 1998; Sugiura et al., 2000]), which was biochemically shown to contain the editing activity to hydrolyze the incorrectly formed aminoacyl-tRNA (Lin et al., 1996). For IleRS, we have reported the crystal structures of *Thermus thermophilus* IleRS complexed with L-isoleucine and with L-valine, which substantiated the mechanism of the "double-sieve" amino acid selection (Nureki et al., 1998). Actually, the first sieve, which accommodates both L-isoleucine and L-valine, was identified on the aminoacylation domain, while the second, editing sieve, which is specific to L-valine, was found to exist on the CP domain, which protrudes from the aminoacylation domain (Nureki et al., 1998). As the aminoacylation and editing reactions are carried out in the two distinct catalytic sites, which are separated by about 35 Å, it remains to be clarified how the valyl moieties of Val-AMP and Val-$tRNA^{Ile}$ are transported from the aminoacylation site to the editing site. Recently, Silvian et al. (1999) determined the crystal structure of *Staphylococcus aureus* IleRS complexed with *E. coli* $tRNA^{Ile}$ and the antibiotic mupirocin. They proposed a shuttling mechanism, in which the valyl moiety of Val-$tRNA^{Ile}$ is transferred from the aminoacylation site to the editing site by a simple bending of the 3′-terminal acceptor strand of $tRNA^{Ile}$, analogous to the editing by DNA polymerase. However, in the reported *S. aureus* IleRS complex structure, the two terminal nucleotides are disordered, due to the lack of interaction between the CCA end and the editing domain (Silvian et al., 1999). Therefore, it is not known how the valylated CCA end is held by the editing domain. Moreover, the structural mechanisms of Val-AMP transport from the aminoacylation site to the distant editing site remain to be elucidated. In contrast to IleRS, the double-sieve mechanism for the discrimination of L-valine from isosteric L-threonine by ValRS has not been elucidated from a structural point of view. In the present study, we have determined the crystal structure of *T. thermophilus* ValRS complexed with $tRNA^{Val}$ and a Val-AMP analog at 2.9 Å resolution, and have elucidated how this protein·RNA complex achieves the sophisticated "double-sieve" discrimination of L-valine from L-isoleucine and L-threonine.

## Results and Discussion

### Structure Determination

*Thermus thermophilus* ValRS is a monomeric enzyme consisting of 862 amino acid residues. The *T. thermophilus* $tRNA^{Val}$ isoacceptor with the CAC anticodon consists of 75 nucleotides. An intermediate analog used in this study is *N*-(L-valyl)-*N*′-adenosyl-diaminosulfone (designated hereafter as Val-AMS). The crystals belong to the space group $P4_22_12$ with unit cell parameters of $a = b = 411.8$ Å, $c = 81.97$ Å, and contain one dimeric complex per asymmetric unit. The structure was solved by multiple isomorphous replacement with anomalous scattering (MIRAS) using platinum and gold derivatives. Density modification by solvent flattening, histogram matching, and 2-fold noncrystallographic symmetry averaging improved the electron density map enough for model building. The model of (ValRS·$tRNAc^{Val}$·Val-AMS)$_2$ was built and refined to 2.9 Å resolution with an *R*-factor of 24.5% ($R_{free}$ = 27.2%) (Table 1). In the present crystal structure, the C-terminal coiled-coil domains of the two ValRS·$tRNA^{Val}$·Val-AMS complexes contact each other (data not shown). In this paper, we discuss only one of the two complexes because the two complexes are geometrically almost identical. Domain architecture of the *T. thermophilus* ValRS is shown in Figure 2. The 3′-end of $tRNA^{Val}$ is bound to the CP-1 domain, as described below. The details of the other specific ValRS··$tRNA^{Val}$ interactions will be described elsewhere.

### Recognition of the Valyl-Adenylate Analog at the Aminoacylation Site, which Serves as the First Sieve

The Val-AMP analog (Val-AMS), in which the –O–P–O– linkage between the valyl and ribose moieties is replaced by –NH–S–NH–, is tightly bound in a deep catalytic cleft of the central Rossmann-fold domain of ValRS (Figure 2). The catalytic cleft of the Rossmann-fold domain serves as the first sieve in the double-sieve substrate selection. First, the α-$NH_3^+$ group of the aminoacyl

Table 1. Crystallographic Data and Refinement Statistics

| Diffraction Data | | | | |
|---|---|---|---|---|
| Crystal | Native | $K_2PtCl_4$ | $NaAuCl_4$ (I) | $NaAuCl_4$ (II) |
| X-ray source | BL41XU SPring8 | BL41XU SPring8 | BL44B2 SPring8 | UltraX18 Rigaku |
| Resolution (Å) | 2.9 | 3.0 | 3.3 | 6.0 |
| Unique reflections | 151,446 | 129,961 | 103,422 | 15,310 |
| Total reflections | 551,728 | 571,204 | 549,448 | 54,681 |
| $R_{merge}$ (%)[2] | 10.0 (32.8)[1] | 8.1 | 8.8 | 8.0 |
| Completeness (%) | 96.4 (85.6)[1] | 90.0 | 98.1 | 84.0 |
| **Phasing Statistics (50–3.0 Å)** | | | | |
| $R_{der}$ (%)[3] | | 12.4 | 11.9 | 19.9 |
| Overall phasing power[4] | | 2.20/1.09 | 0.70/0.48 | 1.05/0.73 |
| $R_{cullis}$[5] | | 0.84 | 0.97 | 0.90 |
| **Refinement Statistics** | | | | |
| Resolution (Å) | 30–2.9 | | | |
| Number of reflections | 150,205 | Rmsd bond lengths (Å) | | 0.008 |
| Number of protein atoms | 13,940 | Rmsd bond angles (°) | | 1.40 |
| Number of RNA atoms | 3,206 | Rmsd impropers (°) | | 1.12 |
| Number of hetero atoms | 64 | | | |
| Number of water molecules | 158 | $R_{work}/R_{free}$ (%)[6] | | 24.5/27.2 |

[1] Numbers in parentheses correspond to the values in the highest resolution shell.
[2] $R_{merge} = \Sigma_h\Sigma_i|I_{hi}-<I_h>|/\Sigma_h\Sigma_i|I_{hi}|$, where $h$ are unique reflection indices, and $i$ indicates symmetry equivalent indices.
[3] $R_{der} = \Sigma||F_{PH}|-|F_P||/\Sigma|F_P|$, where $|F_P|$ and $|F_{PH}|$ refer to the measured structure factor amplitudes of the native and the derivative, respectively.
[4] Phasing power is $f_{rms}/E_{rms}$, where $f_{rms} = [(\Sigma f_H^2)/n]^{1/2}$ and $E_{rms} = [\Sigma(F_{PH} - |F_P + F_H|)^2/n]^{1/2}$.
[5] $R_{cullis} = \Sigma||F_H - (F_{PH} - F_P)|/\Sigma|F_{PH} - F_P|$ (only for centric reflections), where $F_H$ represents the calculated heavy atom structure factor.
[6] $R_{work} = \Sigma|F_O - F_C|/\Sigma F_O$ for reflections of work set, and $R_{free} = \Sigma|F_O - F_C|/\Sigma F_O$, for reflections of test set (5% of total reflections).

moiety of Val-AMS provides three hydrogen bonds with the α-CO group of Pro$^{42}$, the γ-COO$^-$ group of Asp$^{81}$, and the γ-CO group of Asn$^{44}$ (Figure 3A). Second, the aliphatic side chain of the valyl moiety fits into a hydrophobic pocket consisting of Pro$^{41}$, Pro$^{42}$, Trp$^{456}$, Ile$^{491}$, and Trp$^{495}$ of ValRS (Figure 3A). The β-CH group contacts

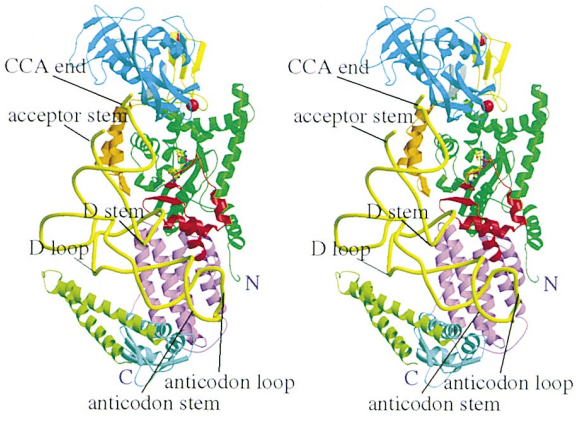


Figure 2. Overview of the Crystal Structure of the *T. thermophilus* ValRS·tRNA$^{Val}$·Val-AMS Ternary Complex

The ValRS structure has six major domains: the Rossmann fold (colored in green), the connective polypeptide (CP) domain (CP core, white; CP-1, cyan; CP-2, orange; CP-3, yellow), the "stem-contact (SC)"-fold domain (red), the "anticodon-loop binding" α-helix bundle domain (magenta), the "anticodon-stem binding" junction domain (light blue), and the "D and T loops binding" C-terminal coiled-coil domain (light green). Two $Zn^{2+}$ ions (shown as red balls) are bound to the Zn-finger structures, respectively, consistent with the previous biochemical study (Kohda et al., 1984). Val-AMS (shown as a ball and stick model) is bound on the aminoacylation domain. The bound tRNA$^{Val}$ is shown as the backbone worm colored in yellow.

both of the Trp$^{456}$ and Ile$^{491}$ side chains: the γ1-$CH_3$ group contacts the Pro$^{41}$ side chain, and the γ2-$CH_3$ group contacts the Pro$^{42}$ and Trp$^{495}$ side chains (Figure 3B). It is impossible to fit an isoleucyl moiety into this pocket, because there is no room for the additional δ-$CH_3$ group between the γ1-$CH_2$ group and the Pro$^{41}$ side chain. These seven binding residues are completely conserved among all ValRSs, except that Asn$^{44}$ is not conserved in the archaeal ValRSs. In the structure of the *T. thermophilus* IleRS complexed with the isoleucyl-adenylate (Ile-AMP) analog (*N*-(L-isoleucyl)-*N*′-adenosyl-diaminosulfone, designated hereafter as Ile-AMS) (Nakama et al., unpublished results), some of the features of the Val-AMS recognition by ValRS are characteristically different, but the rest are well conserved. The amino acid binding pocket in the aminoacylation site of the *T. thermophilus* IleRS involves Gly$^{45}$, Pro$^{46}$, Asp$^{85}$, Trp$^{518}$, Glu$^{550}$, Gln$^{554}$, and Trp$^{558}$ (Figure 3C). These seven residues are absolutely conserved in IleRSs. Among them, Pro$^{46}$, Asp$^{85}$, Trp$^{518}$, and Trp$^{558}$ correspond to the ValRS residues Pro$^{42}$, Asp$^{81}$, Trp$^{456}$, and Trp$^{495}$, respectively (Figures 3A and 3C). The γ-COO$^-$ group of Asp$^{85}$ does not hydrogen bond with the α-$NH_3^+$ group of the aminoacyl moiety of Ile-AMS in the IleRS·Ile-AMS complex structure, but rather bonds with that of L-isoleucine in the previously-reported IleRS·L-isoleucine complex structure (Nureki et al., 1998). On the other hand, the ε-$NH_2$ group of the IleRS-specific Gln$^{554}$ residue forms a hydrogen bond with the α-CO group of the aminoacyl moiety of Ile-AMS. The β-CH, γ1-$CH_2$, and γ2-$CH_3$ groups of the isoleucyl moiety contact the side chains of Gln$^{554}$, Gly$^{45}$, and Trp$^{518}$/Trp$^{558}$, respectively (Figure 3D). The δ-$CH_3$ group, characterizing the isoleucyl moiety, contacts the γ-$CH_2$ moiety of Glu$^{550}$, which serves as the bottom of the pocket (Figure 3D). The pocket of IleRS is wider and deeper than that

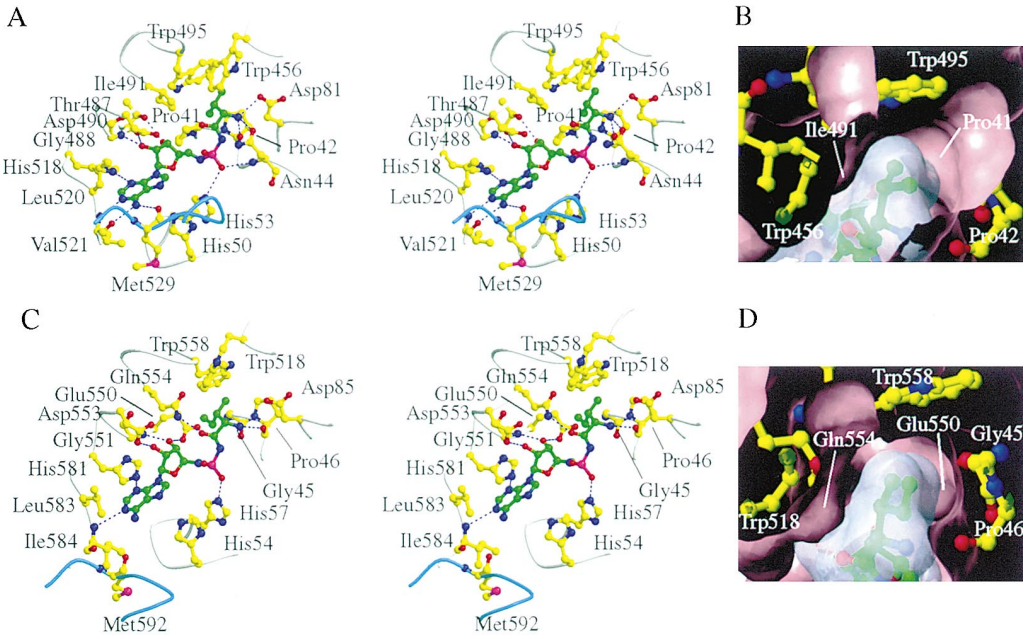


Figure 3. The Aminoacylation Site Serves as the First Sieve

(A) Ball and stick representation of Val-AMS bound on the aminoacylation domain of ValRS (stereo view). The KMSKS loop is colored in cyan. Blue dashed lines indicate hydrogen bonds between Val-AMS and ValRS.

(B) Contact-surface representation of Val-AMS bound on the aminoacylation domain of ValRS.

(C) Ball and stick representation of Ile-AMS bound on the aminoacylation domain of IleRS (stereo view). The manners of presentation are the same as in Figure 2A.

(D) Contact-surface representation of Ile-AMS bound on the aminoacylation domain of IleRS.

of ValRS, mainly because of the replacement of the ValRS Pro$^{41}$ by the IleRS Gly$^{45}$ (Figures 3B and 3D). Therefore, the isoleucyl moiety is located appreciably deeper in the IleRS pocket than the valyl moiety is in the ValRS pocket (Figures 3B and 3D). Thus, the hydrophobic pocket of ValRS excludes L-isoleucine and larger amino acids, and snugly fits L-valine with respect to both its size and shape (Figures 3A and 3B). Nevertheless, the isosteric L-threonine may fit into the pocket of ValRS (Figure 3B). These features agree with the concept of the first, size-based sieve in the double-sieve mechanism of ValRS (Figure 1) (Fersht, 1985). On the other hand, IleRS and ValRS recognize the adenosyl moiety in a similar manner, except for the 6-$NH_2$ group (Figures 3A and 3C). The KMSKS loop of ValRS interacts with the adenosyl moiety, through the hydrogen bond between the $\alpha$-CO group of Met$^{529}$ and the adenine 6-$NH_2$ group (the "closed" form), while that of IleRS is far away from the adenosyl moiety (the "open" form). The closed form of the "KMSKS" loop in the *T. thermophilus* ValRS·tRNA$^{Val}$·Val-AMS structure is well conserved in the *T. thermophilus* LeuRS·Leu-AMS structure (Cusack et al., 2000) and in the *E. coli* GlnRS·tRNA$^{Gln}$·ATP and GlnRS·tRNA$^{Gln}$·Gln-AMS structures (Rould et al., 1989; Rath et al., 1998). It is likely that the KMSKS loop in the closed form may prevent ATP and aminoacyl-adenylate from entering or leaving the binding pocket. On the other hand, the open form of the KMSKS loop is observed in the ligand free and Ile-AMS bound *T. thermophilus* IleRS (Nureki et al., 1998; Nakama et al., unpublished results), as well as in the ligand free *E. coli* and *T. thermophilus* MetRSs (Mechulam et al., 1999; Sugiura et al., 2000). The substrates for aminoacyl-adenylate synthesis can bind to the catalytic site much more easily with the open form KMSKS loop than with the closed form loop. The KMSKS loop appears to be able to change its conformation between the closed and open forms, without steric hindrance by tRNA, in the *T. thermophilus* ValRS complex structure. The role of the conformational change of the KMSKS loop in Thr-AMP and Val-AMP hydrolysis by ValRS and IleRS, respectively, is discussed below.

### Specific Interaction of the 3′-Terminal Adenosine with the Editing Site, which Serves as the Second Sieve

The overall structure of the tRNA bound ValRS exhibits significant geometrical similarity with that of the *T. thermophilus* IleRS in a tRNA free state with an rmsd of 2.89 Å over 608 residues. Most of the domains are superimposable between the two protein structures. The editing domain, CP-1, of the *T. thermophilus* ValRS is arranged in a similar position as that of the *T. thermophilus* IleRS, and the editing active site is 37 Å away from the aminoacylation site in the present structure (Figure 2). The enzyme bound tRNA$^{Val}$ has an L-shaped structure, like the enzyme free tRNA$^{Phe}$ (Sussman and Kim, 1976), with an angle formed by the acceptor and anticodon arms of about 90° (Figure 2). The 3′ terminal strand of tRNA$^{Val}$ extends straight to the editing domain, and is bound in the deep cleft formed by the protruding $\beta$-ribbon and the $\beta$-barrel structure (Figures 2, 4A, and 4B). Concomitantly, the G1·C72 base pair of tRNA$^{Val}$ is

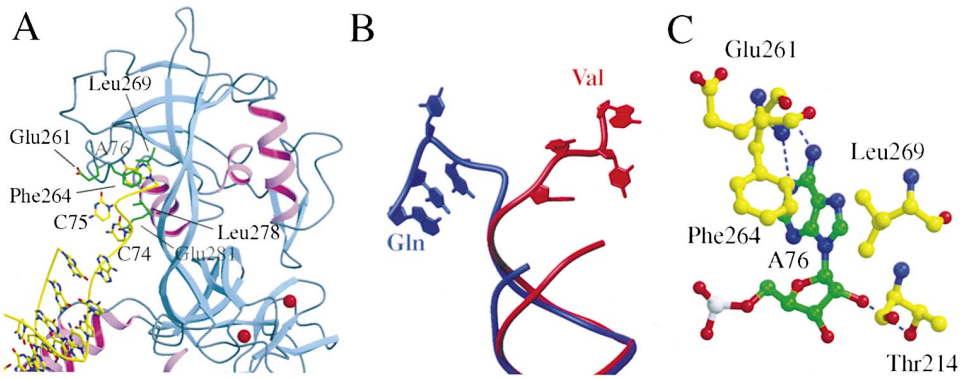


Figure 4. The Editing Site Serves as the Second Sieve

(A) The tRNA$^{Val}$ CCA region is bound to the editing domain. The residues that contact the CCA region are shown as green sticks.

(B) Two distinct conformations of the 3′-terminal strands of tRNA$^{Gln}$ (blue) and tRNA$^{Val}$ (red) in the enzyme bound state. The nucleosides in positions 73–76 are shown as plates.

(C) Specific 3′-A (A76) recognition by the editing domain of ValRS. Blue dashed lines indicate hydrogen bonds between the 3′-A and the editing domain.

disrupted in this ValRS bound structure (Figure 4A). The extended 3′-terminal strand of tRNA$^{Val}$ contrasts sharply with the folded-back strand of tRNA$^{Gln}$ in the aminoacylation complex of *E. coli* GlnRS (Rould et al., 1989; Rath et al., 1998) (Figure 4B).

The 3′-terminal strand of tRNA$^{Val}$ is held primarily by interactions with the protein. The cytosine base of C74 contacts the side chains of Leu$^{278}$ and Glu$^{281}$, while the base and ribose moieties of C75 contact the side chains of Glu$^{261}$ and Phe$^{264}$, respectively (Figure 4A). The 3′-terminal adenosine, A76, is more specifically recognized by the editing domain. The 5′-phosphate group of A76 forms a hydrogen bond with the side chain of Tyr$^{337}$ (not shown). The adenine base of A76 is sandwiched between the side chains of Phe$^{264}$ and Leu$^{269}$ through van-der-Waals contacts (Figure 4C). The N1 atom and 6-$NH_2$ group of A76 form hydrogen bonds with the $\alpha$-NH and $\alpha$-CO groups, respectively, of Glu$^{261}$ (Figure 4C). These amino acid residues involved in the 3′-terminal A76 recognition are highly conserved among ValRSs. The base-specific recognition of A76 is consistent with the previous biochemical result that *E. coli* ValRS exhibited much lower hydrolytic editing activities with Thr-tRNA$^{Val}$ variants with the 3′-terminal A76 replaced by C, G, and U (Tamura et al., 1994). Furthermore, the 2′-OH group of A76 forms a hydrogen bond with the $\gamma$-OH group of Thr$^{214}$ (Figure 4C). Thus, the present complex structure is likely to represent the interaction of ValRS with tRNA$^{Val}$ at the posttransfer editing step for the Thr-tRNA$^{Val}$ hydrolysis.

To compare ValRS and IleRS, the structure of the *T. thermophilus* ValRS editing domain with the bound CCA end of tRNA$^{Val}$ was superposed on that of the *T. thermophilus* IleRS editing domain (Nureki et al., 1998) (rmsd 1.75 Å over 157 residues). The aforementioned A76-interacting elements of ValRS (Figure 4C) are spatially conserved in the IleRS structure; the side chains of the invariant Thr$^{214}$, Phe$^{264}$, and Leu$^{269}$ of ValRS spatially correspond to those of Thr$^{228}$, Trp$^{227}$, and Val$^{318}$, respectively, of IleRS, and the main chain of the ValRS Glu$^{261}$ is superposable on that of the IleRS Ser$^{310}$. Thus, the 3′-terminal A76 residue was fitted into the corresponding site in the IleRS structure without any modification (Figure 5A). Therefore, this suggests that A76 is recognized in the same manner by the IleRS and ValRS editing domains (Figures 5A and 5B).

As for the *T. thermophilus* IleRS, the structures of the complexes of IleRS with L-isoleucine and L-valine were reported in addition to that of IleRS in the free state (Nureki et al., 1998). The electron density of L-valine was observed not only on the Rossmann-fold aminoacylation domain but also on the editing domain of the *T. thermophilus* IleRS (Nureki et al., 1998). We observed two additional electron densities on the editing domain in an initially refined |Fo-Fc| map. In the atomic model reported in Nureki et al. (1998), the two electron densities were assigned to L-valine and water molecules, respectively, as shown previously. The reverse assignment was also possible, and gave an omit map (Nureki et al., 1998), where the L-valine molecule is located in close proximity to the 2′-OH group of the A76 residue fitted on the IleRS structure (Figure 5A). The $\alpha$-$NH_3^+$ group hydrogen bonds with the $\delta$-O of Asp$^{328}$ and the $\alpha$-CO of His$^{319}$, and the $\alpha$-$COO^-$ group hydrogen bonds with the $\gamma$-OH groups of Thr$^{228}$ and Thr$^{230}$, respectively (Figure 5A). The side chain of L-valine is surrounded by the side chains of Thr$^{233}$, His$^{319}$, and Ala$^{321}$, and the main chains of Phe$^{324}$ and Gly$^{325}$ of the IleRS. In other IleRSs, Thr$^{230}$, Thr$^{233}$, His$^{319}$, and Asp$^{328}$ are completely conserved, and Ala$^{321}$ is conserved or replaced by Ser. The pocket is just as large as L-valine, but is too small for L-isoleucine. An additional $CH_3$ group of L-isoleucine clashes with the main chain of Phe$^{324}$ or the side chain of Asp$^{328}$. A slight rotation of the $\alpha$-$COO^-$ group around the $C_\alpha$-CO bond of the bound L-valine molecule allows the covalent linkage of the $\alpha$-CO group of L-valine to the OH group of the modeled A76 moiety (Figure 5A). Therefore, the valine binding pocket near the A76 binding site on the IleRS editing domain is concluded to be for the posttransfer editing, to hydrolyze Val-tRNA$^{Ile}$. The previously reported valine binding pocket of IleRS is discussed below with respect to the pretransfer editing.

On the other hand, in the *T. thermophilus* ValRS structure, Arg$^{216}$, Thr$^{219}$, Lys$^{270}$, Thr$^{272}$, Asp$^{276}$, and Asp$^{279}$ are

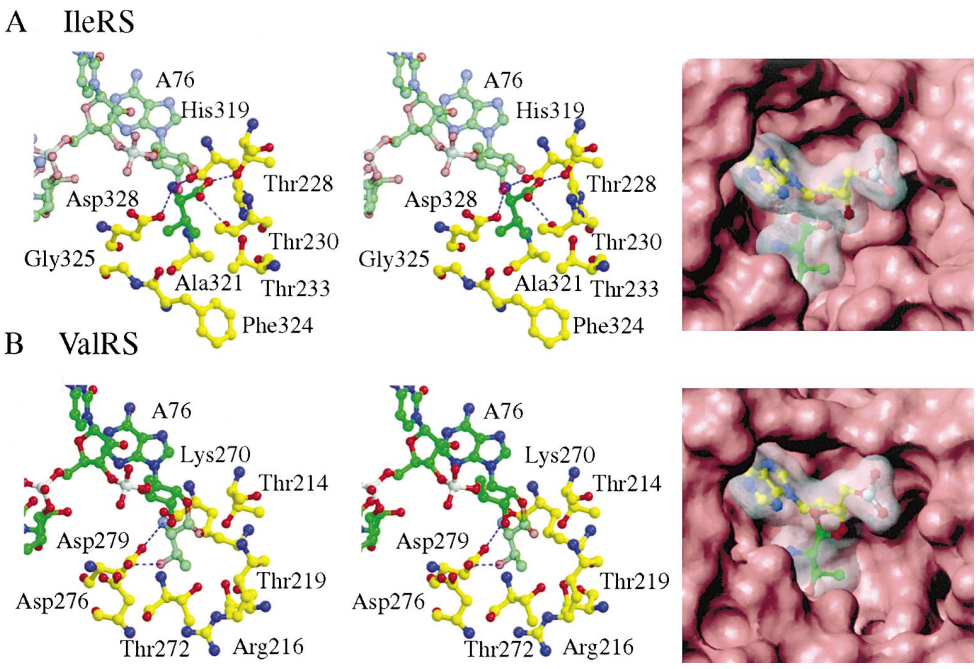


Figure 5. The Posttransfer Editing

(A) Interactions of the Val-tRNA$^{Ile}$ with the IleRS editing domain at the posttransfer editing step. *Left*, a ball and stick representation (stereo view). The amino acid residues constituting the Val binding pocket of the IleRS editing site and the bound L-valine molecule are shown with their carbon atoms colored in yellow and green, respectively. Onto this real structure, the CCA end of tRNA$^{Val}$ was modeled, as shown translucently with the carbon atoms colored in green. *Right*, a contact-surface representation of the bound L-valine (a translucent surface together with a ball and stick representation with the carbon atoms colored in green), A76 (a translucent surface together with a ball and stick representation with the carbon atoms colored in yellow), and the IleRS editing domain (brown).

(B) Interactions of the Thr-tRNA$^{Val}$ with the ValRS editing domain at the posttransfer editing step. *Left*, a ball and stick representation (stereo view). The amino acid residues constituting the Thr binding pocket of the ValRS editing site and the bound tRNA$^{Val}$ are shown with their carbon atoms colored in yellow and green, respectively. Onto this real structure, L-threonine was modeled, as shown translucently with the carbon atoms colored in green. *Right*, a contact-surface representation of Thr-A76 (a translucent surface together with ball and stick representations of the Thr and adenylyl moieties with the carbon atoms colored in green and yellow, respectively) and the ValRS editing domain (brown).

near the A76 binding site (Figure 5B), and form a more hydrophilic pocket, which spatially corresponds to the pocket for L-valine of the IleRS editing domain. These amino acid residues are strictly conserved in ValRSs. We manually fitted L-threonine into the ValRS pocket, in a manner similar to the binding of L-valine to the posttransfer editing pocket of IleRS. The Asp$^{279}$ side chain of ValRS protrudes into the pocket, as compared with that of the corresponding Asp$^{328}$ residue in the *T. thermophilus* IleRS. Thus, to avoid steric clash with the threonine molecule, the $\gamma$-COO$^-$ group of Asp$^{279}$ was rotated by 4° around the $C_\alpha$–$C_\beta$ bond, and by 54° around the $C_\beta$–$C_\gamma$ bond. In this model, the $\alpha$-CO group of the L-threonine is covalently bonded to the 2′-OH group of A76, and the $\alpha$-$NH_3^+$ group forms a hydrogen bond with the $\delta$2-O atom of Asp$^{279}$ (Figure 5B). As for the side chain of the threonyl moiety, the $\gamma$-OH group also forms a hydrogen bond with the $\delta$1-O atom of Asp$^{279}$, while the $\gamma$-$CH_3$ group is sandwiched between the $\beta$-$CH_2$ of Arg$^{216}$ and the $\epsilon$-$CH_2$ of Lys$^{270}$. In addition, the $\gamma$-OH group may be recognized by the ValRS-characteristic Asp$^{276}$. A valyl moiety should be precluded from fitting into this pocket because of the lack of proper hydrogen bonding with the $\delta$-O atom of Asp$^{279}$. In contrast, the aminoacyl moieties of cysteinyl-tRNA$^{Val}$ and $\alpha$-aminobutyryl-tRNA$^{Val}$ may be accepted and hydrolyzed, because they are smaller than that of Val-tRNA$^{Val}$ by one $CH_3$ group.

The present ValRS complex structure reveals that, at the posttransfer editing step, the second sieve of ValRS distinguishes L-threonine from L-valine based on the characteristic $\gamma$-OH group, whereas that of IleRS discriminates L-valine from L-isoleucine based primarily on the size. The comparison of the posttransfer editing sites between ValRS and IleRS demonstrates that a similar hydrolytic reaction accompanies the different manners of substrate selection.

### Comparison between the tRNA-Complexed IleRS and ValRS Structures

In the *S. aureus* IleRS complex structure, the 3′ end of tRNA$^{Ile}$ is not bound in the aminoacylation site (Silvian et al., 1999). Moreover, although the 3′ terminal acceptor strand of tRNA$^{Ile}$ projects toward the editing domain, C75 and A76 are structurally disordered, probably because of the lack of interaction between the CCA end and the editing domain (Silvian et al., 1999). Correspondingly, it was also reported that the IleRS editing domain is worse ordered than other domains (Silvian et al., 1999). The editing domain of the *S. aureus* IleRS complex is rotated by about 47° (Silvian et al., 1999) as compared with that of the tRNA free *T. thermophilus* IleRS (Nureki et al., 1998). Therefore, in modeling the missing 3′ CA of tRNA$^{Ile}$, as reported by Silvian et al. (1999), the 3′

terminal adenosine cannot reach the editing active site described above. Thus, the *S. aureus* IleRS complex structure does not represent the Val-tRNA$^{Ile}$ hydrolysis. In contrast, the editing domain of the *T. thermophilus* ValRS is arranged in a similar position as that of the tRNA free *T. thermophilus* IleRS, and can hold the 3′ CCA end of tRNA$^{Val}$, representing the interaction of ValRS with tRNA$^{Val}$ for the Thr-tRNA$^{Val}$ hydrolysis (Figures 2 and 4A). Therefore, the editing domain can adopt two distinct orientations in the tRNA-complexed state. The two orientations are designated hereafter as "orientations I and II": orientation I corresponds to the editing domains of the tRNA free *T. thermophilus* IleRS and the tRNA bound *T. thermophilus* ValRS, while orientation II corresponds to that of the *S. aureus* IleRS complex. Comparison of the tRNA free *T. thermophilus* IleRS, tRNA bound *S. aureus* IleRS, and tRNA bound *T. thermophilus* ValRS structures reveals that the two different orientations of the editing domain are due to the conformational difference at the hinge connecting it to the CP core (Figure 6A). Actually, this hinge is observed in the corresponding position in the *E. coli* and *T. thermophilus* MetRSs, which also possess much smaller CP-1 subdomains than those of IleRS and ValRS (Mechulam et al., 1999; Sugiura et al., 2000). In these two MetRS structures, the CP-1 orientations are different (Figure 6A). In solution, the different CP-1 orientations may be similarly stable.

In the present *T. thermophilus* ValRS complex structure, the editing domain adopts orientation I, and prevents the 3′ end of tRNA$^{Val}$ from approaching and entering the aminoacylation site (Figures 6B and 6D). However, if the editing domain of ValRS adopts orientation II, then the 3′ terminal acceptor strand of tRNA$^{Val}$ can simply fold back (Figures 6B and 6C), as observed for *E. coli* tRNA$^{Gln}$ (Rould et al., 1989) (Figure 4B), without steric hindrance with the polypeptide chain of the enzyme, and enter the aminoacylation site. A model structure of ValRS·tRNA$^{Val}$ at the aminoacylation step was built by combining nucleotides 1–69 of *T. thermophilus* tRNA$^{Val}$ and nucleotides 70–76 of *E. coli* tRNA$^{Gln}$, after superposition of *E. coli* tRNA$^{Gln}$ on *T. thermophilus* tRNA$^{Val}$ on the basis of the acceptor-stem and anticodon–stem structures. No further modification was necessary. In this aminoacylation model structure of the ValRS complex, the 2′-OH group of A76 is positioned close to the $\alpha$-CO group of the valyl moiety of Val-AMS. In the *S. aureus* IleRS complex structure (adopting orientation II), a similar aminoacylation model was also bulit, but some modification was required (Silvian et al., 1999). In the *S. aureus* IleRS complex structure, the long carboxylate tail of mupirocin bound in the aminoacylation site pushed the KMSKS loop more open than usual, and the concomitant steric hindrance between the KMSKS loop and the tRNA$^{Ile}$ D stem appeared to have caused the extraordinary positioning of the tRNA$^{Ile}$ (Protein Data Bank accession code 1QU2).

### The Pretransfer Editing

Several biochemical studies have suggested that the sites for aminoacylation and editing are separate in IleRS (Schmidt and Schimmel, 1994; Farrow et al., 1999; Nomanbhoy et al., 1999) and ValRS (Lin and Schimmel, 1996; Nomanbhoy and Schimmel, 2000). Actually, the editing domains of IleRS and ValRS have the posttransfer editing activity by themselves (Lin et al., 1996), and an IleRS mutant [$\Delta$(219 to 265)] that lacks 47 amino acid residues in the editing domain cannot hydrolyze Val-tRNA$^{Ile}$ (Nureki et al., 1998). Hence, the editing domain has been proven to be responsible for the posttransfer editing. In addition, we have reported that a single point mutation, either T243A or N250A, in the *E. coli* IleRS editing domain completely abolishes the editing activity for both Val-AMP and Val-tRNA$^{Ile}$ hydrolysis (Nureki et al., 1998). This study indicates that the editing domain of IleRS is also responsible for the pretransfer editing. However, in contrast to the case of the posttransfer editing, it remains unclear how an incorrectly synthesized aminoacyl-adenylate is transferred from the aminoacylation site to the editing site. As for the pretransfer editing of the Val-AMP by IleRS, Silvian et al. (1999) pointed out that a channel spans the aminoacylation site and the editing site in the *S. aureus* IleRS complex structure, and implied that a Val-AMP molecule diffuses from the aminoacylation site to the editing site through the channel at the pretransfer editing step ("the diffusion model"). Furthermore, with respect to the tRNA-dependency of the pretransfer editing, it was suggested that the opening of the KMSKS loop might be promoted by the binding of tRNA$^{Ile}$ and might result in easier release of Val-AMP from the aminoacylation site (Silvian et al., 1999).

On the other hand, in the present *T. thermophilus* ValRS complex, the closed form of the KMSKS loop covers the aminoacylation site, just like the flap of a pocket (Figure 3A), and the corresponding channel is blocked by the long $\beta$-ribbon structure of the editing domain (Figure 6D) due to the editing domain in orientation I. Around the aminoacylation site, there are no more than two small rooms: one is for the $\beta$- and $\gamma$-phosphates of ATP, and the other is for the 3′-A of tRNA$^{Val}$. However, if the editing domain of ValRS adopts orientation II, then the channel is formed (Figures 6E and 6F), suggesting that the translocation of the Thr-AMP by the ValRS·tRNA$^{Val}$ complex occurs in a similar manner as that of the Val-AMP by the IleRS·tRNA$^{Ile}$ complex. In addition, as we pointed out above, with the other conformation, the open form of the KMSKS loop, the Thr-AMP molecule can leave the aminoacylation site for the pretransfer editing site of the ValRS editing domain. As far as the present ValRS·tRNA complex structure is concerned, opening/closing of the KMSKS loop does not seem to be tRNA-dependent. Nevertheless, the diffusion model may explain the tRNA-dependency of the pretransfer editing, because the channel is composed of both ValRS and tRNA. As for tRNA$^{Ile}$, three nucleotide residues, and probably their posttranscriptional modifications, in the D loop are important for the editing by IleRS (Hale et al., 1997; Farrow et al., 1999), although this region of tRNA is not involved in the interaction with IleRS (Silvian et al., 1999). As the D loop is involved in tertiary interactions with the T loop, it is possible that the proper L-shaped tertiary structure retained by the loop–loop interactions is required for the tRNA-dependent pretransfer editing.

At the end of the channel on the ValRS·tRNA$^{Val}$ complex, we can find the posttransfer editing site described above. If the threonyl moieties of Thr-AMP and Thr-

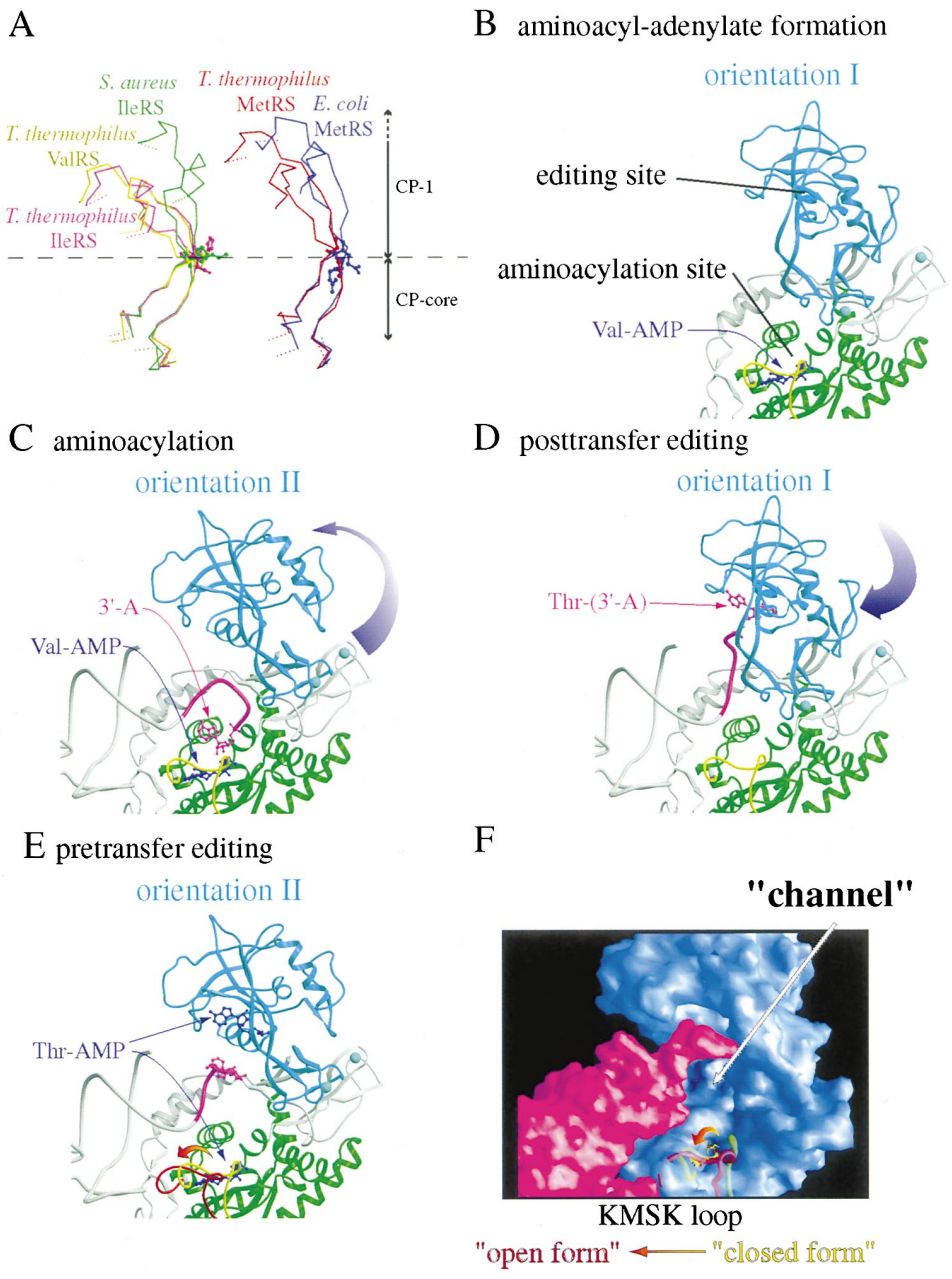


Figure 6. The "Double-Sieve" Amino Acid Selection by ValRS

(A) A Cα-trace representation around the "hinges" in the *S.aureus* IleRS (green), the *T. thermophilus* IleRS (magenta), the *T. thermophilus* ValRS (yellow), the *E. coli* MetRS (blue), and the *T. thermophilus* MetRS (red). The *S.aureus* IleRS and the *T. thermophilus* ValRS are tRNA bound, while the *T. thermophilus* IleRS, the *E. coli* MetRS (blue), and the *T. thermophilus* MetRS are tRNA free. For each of these synthetases, the two amino acid residues on the boundary between the CP-1 subdomain and the CP core are shown in a ball and stick representation.

(B) The aminoacyl-adenylate synthesis. Larger L-isoleucine is precluded, but isosteric L-threonine, smaller L-cysteine, and L-α-aminobutyrate may be accepted in addition to the cognate L-valine. The KMSKS loop in the closed form is colored in yellow. The editing domain is in orientation I.

(C) The aminoacylation of $tRNA^{Val}$. The dark violet arrow represents the rotation of the editing domain from orientation I (B) to orientation II (C), which allows the CCA end (colored in magenta) of $tRNA^{Val}$ to fold back and enter the aminoacylation site. In addition to the valyl moiety of Val−AMP, the aminoacyl moieties of Thr-AMP, cysteinyl-adenylate, and α-aminobutyryl-adenylate may be transferred to the 3′-A of $tRNA^{Val}$. The KMSKS loop in the closed form is colored in yellow.

(D) The posttransfer editing. After the aminoacylation of $tRNA^{Val}$, the aminoacylated 3′-A of $tRNA^{Val}$ is released from the aminoacylation site. The dark violet arrow represents the rotation of the editing domain from orientation II (C) to orientation I (D). Then, the threonylated, cysteinylated, or α-aminobutyrylated 3′-A (but not the valylated 3′-A) of $tRNA^{Val}$ is caught and hydrolyzed by the editing domain in orientation I. Consequently, only the Val-$tRNA^{Val}$ is produced.

(E) The pretransfer editing. Before the transfer of the aminoacyl moiety to the 3′-A of $tRNA^{Val}$ with the editing domain in orientation II (C), the flexible CCA segment may take another conformation with the 3′-A exposed to the solvent (E). Thus, a channel is formed to span the aminoacylation site on the Rossmann-fold domain and the editing site on the editing domain in orientation II. The opening of the KMSKS loop

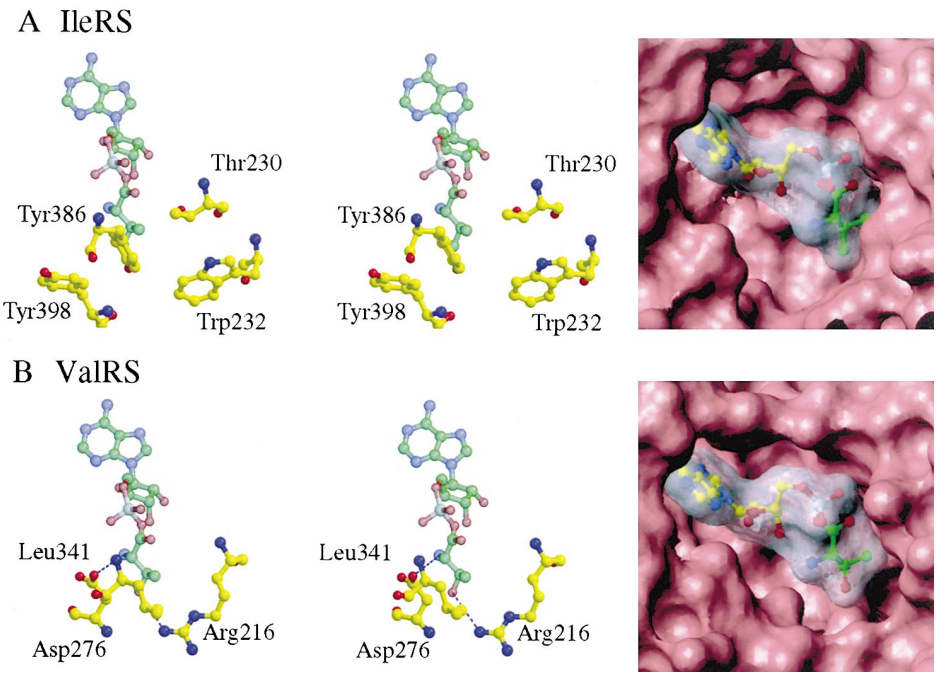


Figure 7. The Pretransfer Editing

(A) A model of Val-AMP at the pretransfer editing step on the IleRS editing domain. *Left*, a ball and stick representation (stereo view). The amino acid residues constituting the Val binding pocket are shown with their carbon atoms colored in yellow. Onto this real structure, Val-AMP is modeled, as shown translucently with the carbon atoms colored in green. *Right*, a contact-surface representation. The editing domain of IleRS is shown in brown. The modeled Val-AMP is shown in a translucent contact-surface representation together with a ball and stick representation (the carbon atoms of the Val moiety are colored in green, while those of the adenylyl moiety are colored in yellow).

(B) A model of Thr-AMP at the pretransfer editing step on the ValRS editing domain. *Left*, a ball and stick representation (stereo view). The amino acid residues constituting the Thr binding pocket are shown with their carbon atoms colored in yellow. Onto this real structure, Thr-AMP is modeled, as shown translucently with the carbon atoms colored in green. *Right*, a contact-surface representation. The editing domain of ValRS is shown in brown. The modeled Thr-AMP is shown in a translucent contact-surface representation together with a ball and stick representation (the carbon atoms of the Thr moiety are colored in green, while those of the adenylyl moiety are colored in yellow).

tRNA$^{Val}$ share the same pocket at both the pretransfer and posttransfer editing steps, then the adenosyl moiety of the Thr-AMP cannot bind to the pocket for that of the Thr-tRNA$^{Val}$. Although the adenosyl moiety can contact the rather flat surface of the cleft in the editing domain, we could not find any pocket to accommodate the adenine ring of the Thr-AMP. On the other hand, if the adenosyl moieties of Thr-AMP and Thr-tRNA$^{Val}$ share the same pocket, then we can easily find a pocket for the threonyl-moiety of the Thr-AMP, which is near the 5′-$PO_4^-$ group of the 3′-terminal A76 of tRNA$^{Val}$. At the corresponding position in the IleRS editing domain, a hydrophobic pocket has been identified by Nureki et al. (1998). Therefore, we made a docking model of Val−AMP and the IleRS editing domain, and that of Thr-AMP and the ValRS editing domain, which are likely to represent the pretransfer editing step. As shown in Figure 7A, the valine side chain of Val−AMP is fitted into the hydrophobic pocket consisting of Thr$^{230}$, Trp$^{232}$, Tyr$^{386}$, and Tyr$^{398}$ of IleRS, as reported by Nureki et al. (1998). These four residues are conserved or replaced by functionally equivalent residues in IleRSs. In particular, Trp$^{232}$, Tyr$^{386}$, and Tyr$^{398}$ are characteristic of IleRS. The putative pretransfer editing pocket, as well as the posttransfer editing pocket, of IleRS is just as large as the valyl moiety, and thus cannot accommodate the isoleucyl moiety.

On the other hand, in the model of Thr-AMP and the ValRS editing domain (Figure 7B), the $\alpha$-$NH_3^+$ group forms a hydrogen bond with the $\delta$2-O atom of Asp$^{276}$. As for the side chain of the threonyl moiety, the $\gamma$-OH group forms a hydrogen bond with the $\eta$2-$NH_2$ of Arg$^{216}$, while the $\gamma$-$CH_3$ group is sandwiched between the $\gamma$-$CH_2$ of Arg$^{216}$ and the $\alpha$-CH of Leu$^{341}$. A valyl moiety should be precluded from fitting into this pocket, because of the lack of the proper hydrogen bond with the $\eta$2-$NH_2$ of Arg$^{216}$ at the pretransfer editing step. The *T. thermophilus* ValRS Arg$^{216}$ and Asp$^{276}$ are conserved in other ValRSs,

(colored in red) promotes the translocation of Thr-AMP, cysteinyl-adenylate, and $\alpha$-aminobutyryl-adenylate from the aminoacylation site to the editing site through the channel. Due to orientation II of the editing domain, the 3′-A of tRNA$^{Val}$ cannot bind to the adenosyl-moiety binding site in the editing domain. Thus, the editing domain can accept Thr-AMP, cysteinyl-adenylate, and $\alpha$-aminobutyryl-adenylate and hydrolyze them. The arrow represents the KMSKS loop movement from the closed form (yellow) to the open form (red).

(F) A molecular surface representation of the model of the ValRS (blue)· tRNA$^{Val}$ (red) complex in the pretransfer editing state. The open and closed forms of the KMSKS loop are shown as red and yellow backbone worms, respectively. This view highlights the channel spanning the aminoacylation site and the editing site.

as mentioned above, and Leu[341] is conserved or replaced by Val/Ile. The threonyl moiety to be removed by hydrolysis might be discriminated from the valyl moiety by specific recognition of the γ-OH group at the pretransfer editing step as well as the posttransfer editing step. In addition, this putative pretransfer editing pocket of ValRS may accommodate the cysteinyl moiety of cysteinyl adenylate (Jakubowski, 1980; Jakubowski and Fersht, 1981) and the α-aminobutyryl moiety of α-aminobutyryl adenylate (Fersht and Dingwall, 1979; Jakubowski, 1980), because the sizes of their side chains are smaller than that of L-valine by one $CH_3$ group.

On our present assumption, the same adenosyl binding site is utilized at the pretransfer and posttransfer editing steps, while the aminoacyl binding sites are discrete. Actually, the mutations T243A and N250A in *E. coli* IleRS are supposed to affect the posttransfer editing pathway, and furthermore, completely abolish both of the pretransfer and posttransfer editing activities (Nureki et al., 1998).

## Experimental Procedures

### Crystallization

Overproduction and purification of the *T. thermophilus* ValRS were carried out in a similar way as that of the *T. thermophilus* IleRS (Nureki et al., 1998). The *T. thermophilus* $tRNA^{Val}$ isoacceptor with the CAC anticodon was transcribed in vitro with T7 RNA polymerase. Crystals were grown at 4°C by the hanging-drop vapor diffusion method over a period of 2 months. The protein/tRNA solution for crystallization was prepared at a final protein concentration of 7–10 mg/ml for molar ratios of ValRS, tRNA, and Val-AMS of 1:1.1:2. 1 μl of the protein/tRNA solution was mixed with 1 μl of a crystallization solution, 50 mM sodium cacodylate buffer (pH 6.5) containing 1.0 M ammonium sulfate, 10 mM magnesium sulfate, and 6% 1,8-diaminooctane. The drop solution was slowly equilibrated against a reservoir solution, 50 mM sodium cacodylate buffer (pH 6.5) containing 2.8 M ammonium sulfate and 10 mM magnesium sulfate.

### Crystallographic Analysis

For data collection under cryo conditions, the concentration of ethylene glycol in the mother liquor was increased to 23% in three steps (5%, 15%, and 23%) by using micro dialysis before flash cooling. The first two dialysis steps were thirty minutes each and the last step was one hour. All data collections were carried out at 90 K. Native and $K_2PtCl_4$ derivative data sets were collected at station BL41XU, SPring8, Harima, Japan (λ = 0.708 Å). Two $NaAuCl_4$ derivative data sets were collected at station BL44B2, SPring8, Harima, Japan (λ = 1.00 Å) and on a laboratory detection system comprising an R-axisIV image plate in conjunction with mirror-focused CuKα X-rays from a Rigaku rotating anode generator, UltraX18. All of the data sets were processed with the programs DENZO and SCALEPACK (Otwinowski and Minor, 1997). Subsequent phase calculations were carried out with the CCP4 program suite (CCP4, 1994). The structure was solved by multiple isomorphous replacement augmented with anomalous scattering (MIRAS) using three derivatized crystals. Initially, two major heavy atom sites were identified in the difference Patterson map of the platinum derivative. The other platinum sites and the gold sites were identified from cross-difference Fourier maps. Heavy atom refinement and phase calculations were performed with the program MLPHARE (CCP4, 1994). The application of density modification procedures, including solvent flattening (75% estimated solvent), histogram matching, and noncrystallographic symmetry averaging, with the program DM (CCP4, 1994), improved the quality of the phases sufficiently to yield an interpretable electron density map. Iterative model building and density modification with an improved mask greatly enhanced the quality of the electron density map. The model, except the $tRNA^{Val}$ CCA end, was built using the program O (Jones et al., 1991), and was refined by conventional minimization and simulated annealing procedures with the programs XPLOR (Brünger, 1992) and CNS (Brünger et al., 1998). The model of the $tRNA^{Val}$ CCA end was additionally built in a $\sigma_a$-weighted phase combined electron density map after the initial refinement. All measured data within a resolution of 30.0 and 2.9 Å (with the exception of the random 5% of reflections used for the calculation of $R_{free}$) were used in the refinement, during which bulk solvent correction was applied to the reflection data. The Ramachandran plot analysis with the program PROCHECK (Laskowski et al., 1993) showed that 98.0% of the residues in the present structure are in the most favored and additionally allowed regions. Molecular graphics pictures in Figures 1–7 were prepared by using the programs O (Jones et al., 1991), Molmol (Koradi et al., 1996), Molscript (Kraulis, 1991), and Raster3D (Merritt and Bacon, 1997).

### Acknowledgments

We thank Drs. M. Kawamoto, N. Kamiya, S. Adachi, T. Kumasaka, and M. Yamamoto for synchrotron data collection at SPring-8. This work was supported in part by Grants-in-Aid for Scientific Research on Priority Areas (09278101 and 11169204) to S. Y. and O. N., respectively, from the Ministry of Education, Science, Culture and Sports of Japan. S. F. was supported by Research Fellowships of the Japan Society for the Promotion of Science for Young Scientists.

Received July 20, 2000; revised October 6, 2000.

## References

Brünger, A.T. (1992). XPLOR: A System for X-Ray Crystallography and NMR (New Haven, CT: Yale University Press).

Brünger, A.T., Adams, P.D., Clore, G.M., DeLano, W.L., Gros, P., Grosse-Kunstleve, R.W., Jiang, J.S., Kuszewski, J., Nilges, M., Pannu, N.S., et al. (1998). Crystallography & NMR system: A new software suite for macromolecular structure determination. Acta Crystallogr. D Biol. Crystallogr. *54*, 905–921.

CCP4 (Collaborative Computational Project No. 4) (1994). The CCP4 suite: programs for protein crystallography. Acta Crystallogr. D Biol. Crystallogr. *50*, 760–763.

Cusack, S., Yaremchuk, A., and Tukalo, M. (2000). The 2 Å crystal structure of leucyl-tRNA synthetase and its complex with a leucyl-adenylate analogue. EMBO J. *19*, 2351–2361.

Eldred, E.W., and Schimmel, P.R. (1972). Rapid deacylation by isoleucyl transfer ribonucleic acid synthetase of isoleucine-specific transfer ribonucleic acid aminoacylated with valine. J. Biol. Chem. *247*, 2961–2964.

Englisch, S., Englisch, U., von der Haar, F., and Cramer, F. (1986). The proofreading of hydroxy analogues of leucine and isoleucine by leucyl-tRNA synthetases from *E. coli* and yeast. Nucleic Acids Res. *14*, 7529–7539.

Eriani, G., Delarue, M., Poch, O., Gangloff, J., and Moras, D. (1990). Partition of tRNA synthetases into two classes based on mutually exclusive sets of sequence motifs. Nature *347*, 203–206.

Farrow, M.A., Nordin, B.E., and Schimmel, P. (1999). Nucleotide determinants for tRNA-dependent amino acid discrimination by a class I tRNA synthetase. Biochemistry *38*, 16898–16903.

Fersht, A.R. (1977). Editing mechanisms in protein synthesis. Rejection of valine by the isoleucyl-tRNA synthetase. Biochemistry *16*, 1025–1030.

Fersht, A. (1985). Enzyme Structure and Mechanism, Second Edition (New York: W. H. Freeman and Company), pp. 1–475.

Fersht, A.R., and Dingwall, C. (1979). Establishing the misacylation/deacylation of the tRNA pathway for the editing mechanism of prokaryotic and eukaryotic valyl-tRNA synthetases. Biochemistry *18*, 1238–1245.

Fersht, A.R., and Kaethner, M.M. (1976a). Mechanism of aminoacylation of tRNA. Proof of the aminoacyl adenylate pathway for the isoleucyl- and tyrosyl-tRNA synthetases from *Escherichia coli* K12. Biochemistry *15*, 818–823.

Fersht, A.R., and Kaethner, M.M. (1976b). Enzyme hyperspecificity.

Rejection of threonine by the valyl-tRNA synthetase by misacylation and hydrolytic editing. Biochemistry *15*, 3342–3346.

Freist, W., Pardowitz, I., and Cramer, F. (1985). Isoleucyl-tRNA synthetase from bakers' yeast: multistep proofreading in discrimination between isoleucine and valine with modulated accuracy, a scheme for molecular recognition by energy dissipation. Biochemistry *24*, 7014–7023.

Freist, W., Sternbach, H., and Cramer, F. (1994). Threonyl-tRNA synthetase from yeast. Discrimination of 19 amino acids in aminoacylation of tRNA(Thr)-C-C-A and tRNA(Thr)-C-C-A(2' $NH_2$). Eur. J. Biochem. *220*, 745–752.

Giegé, R., Sissler, M., and Florentz, C. (1998). Universal rules and idiosyncratic features in tRNA identity. Nucleic Acids Res. *26*, 5017–5035.

Hale, S.P., and Schimmel, P. (1996). Protein synthesis editing by a DNA aptamer. Proc. Natl. Acad. Sci. USA *93*, 2755–2758.

Hale, S.P., Auld, D.S., Schmidt, E., and Schimmel, P. (1997). Discrete determinants in transfer RNA for editing and aminoacylation. Science *276*, 1250–1252.

Igloi, G.L., von der Haar, F., and Cramer, F. (1977). Hydrolytic action of aminoacyl-tRNA synthetases from baker's yeast. "Chemical proofreading" of Thr-tRNA$^{Val}$ by valyl-tRNA synthetase studied with modified tRNA$^{Val}$ and amino acid analogues. Biochemistry *16*, 1696–1702.

Jakubowski, H. (1980). Valyl-tRNA synthetase from yellow lupin seeds: hydrolysis of the enzyme-bound noncognate aminoacyl adenylate as a possible mechanism of increasing specificity of the aminoacyl-tRNA synthetase. Biochemistry *19*, 5071–5078.

Jakubowski, H., and Fersht, A.R. (1981). Alternative pathways for editing non-cognate amino acids by aminoacyl-tRNA synthetases. Nucleic Acids Res. *9*, 3105–3117.

Jones, T.A., Zou, J.Y., Cowan, S.W, and Kjeldgaard (1991). Improved methods for binding protein models in electron density maps and the location of errors in these models. Acta Crystallogr. A *47*, 110–119.

Kohda, D., Yokoyama, S., and Miyazawa, T. (1984). Thermostable valyl-tRNA, isoleucyl-tRNA and methionyl-tRNA synthetases from an extreme thermophile *Thermus thermophilus* HB8: protein structure and $Zn^{2+}$ binding. FEBS Lett. *174*, 20–23.

Koradi, R., Billeter, M., and Wüthrich, K. (1996). MOLMOL: a program for display and analysis of macromolecular structures. J. Mol. Graph. *14*, 51–55.

Kraulis, P.J. (1991). MOLSCRIPT: A program to produce both detailed and schematic plots of protein structures. J. Appl. Crystallogr. *24*, 946–950.

Laskowski, R.A., MacArthur, M.W., Moss, D.S., and Thornton, J.M. (1993). PROCHECK: a program to check the stereochemical quality of protein structures. J. Appl. Crystallogr. *26*, 283–291.

Lin, L., and Schimmel, P. (1996). Mutational analysis suggests the same design for editing activities of two tRNA synthetases. Biochemistry *35*, 5596–5601.

Lin, L., Hale, S.P., and Schimmel, P. (1996). Aminoacylation error correction. Nature *384*, 33–34.

Mechulam, Y., Schmitt, E., Maveyraud, L., Zelwer, C., Nureki, O., Yokoyama, S., Konno, M., and Blanquet, S. (1999). Crystal structure of *Escherichia coli* methionyl-tRNA synthetase highlights species-specific features. J. Mol. Biol. *294*, 1287–1297.

Merritt, E.A., and Bacon, D.J. (1997). Raster3D. Photorealistic Molecular Graphics. Methods Enzymol. *277*, 505–524.

Nomanbhoy, T.K., and Schimmel, P.R. (2000). Misactivated amino acids translocate at similar rates across surface of a tRNA synthetase. Proc. Natl. Acad. Sci. USA *97*, 5119–5122.

Nomanbhoy, T.K., Hendrickson, T.L., and Schimmel, P. (1999). Transfer RNA-dependent translocation of misactivated amino acids to prevent errors in protein synthesis. Mol. Cell *4*, 519–528.

Nureki, O., Vassylyev, D.G., Tateno, M., Shimada, A., Nakama, T., Fukai, S., Konno, M., Hendrickson, T.L., Schimmel, P., and Yokoyama, S. (1998). Enzyme structure with two catalytic sites for double-sieve selection of substrate. Science *280*, 578–582.

Otwinowski, Z., and Minor, W. (1997). Processing of X-ray diffraction data collected in oscillation mode. Methods Enzymol. *276*, 307–326.

Pauling, L. (1957). The probability of errors in the process of synthesis of protein molecules. In Festschrift Arthur Stroll. (Basel, Switzerland: Birkhäuser-Verlag), pp. 597–602.

Rath, V.L., Silvian, L.F., Beijer, B., Sproat, B.S., and Steitz, T.A. (1998). How glutaminyl-tRNA synthetase selects glutamine. Structure *6*, 439–449.

Rould, M.A., Perona, J.J., Söll, D., and Steitz, T.A. (1989). Structure of *E. coli* glutaminyl-tRNA synthetase complexed with tRNA(Gln) and ATP at 2.8 Å resolution. Science *246*, 1135–1142.

Sankaranarayanan, R., Dock-Bregeon, A.C., Romby, P., Caillet, J., Springer, M., Rees, B., Ehresmann, C., Ehresmann, B., and Moras, D. (1999). The structure of threonyl-tRNA synthetase-tRNA$^{Thr}$ complex enlightens its repressor activity and reveals an essential zinc ion in the active site. Cell *97*, 371–381.

Sankaranarayanan, R., Dock-Bregeon, A.-C., Rees, B., Bovee, M., Caillet, J., Romby, P., Francklyn, C.S., and Moras, D. (2000). Zinc ion mediated amino acid discrimination by threonyl-tRNA synthetase. Nat. Struct. Biol. *7*, 461–465.

Schmidt, E., and Schimmel, P. (1994). Mutational isolation of a sieve for editing in a transfer RNA synthetase. Science *264*, 265–267.

Silvian, L.F., Wang, J., and Steitz, T.A. (1999). Insights into editing from an Ile-tRNA synthetase structure with tRNA$^{Ile}$ and mupirocin. Science *285*, 1074–1077.

Sugiura, I., Nureki, O., Ugaji-Yoshikawa, Y., Kuwabara, S., Shimada, A., Tateno, M., Lorber, B., Giegé, R., Moras, D., Yokoyama, S., and Konno, M. (2000). The 2.0 Å crystal structure of *Thermus thermophilus* methionyl-tRNA synthetase reveals two RNA-binding modules. Structure Fold. Des. *8*, 197–208.

Sussman, J.L., and Kim, S. (1976). Three-dimensional structure of a transfer RNA in two crystal forms. Science *192*, 853–858.

Tamura, K., Nameki, N., Hasegawa, T., Shimizu, M., and Himeno, H. (1994). Role of the CCA terminal sequence of tRNA(Val) in aminoacylation with valyl-tRNA synthetase. J. Biol. Chem. *269*, 22173–22177.

Tsui, W.C., and Fersht, A.R. (1981). Probing the principles of amino acid selection using the alanyl-tRNA synthetase from Escherichia coli. Nucleic Acids Res. *9*, 4627–4637.

**Protein Data Bank ID Code**

The coordinates of the (ValRS·tRNA$^{Val}$·Val-AMS)$_2$ complex structure have been deposited with the ID code 1GAX.